BRNO UNIVERSITY OF TECHNOLOGY
VYSOKÉ UČENÍ TECHNICKÉ V BRNĚ

FACULTY OF CIVIL ENGINEERING
ÚSTAV STAVEBNÍ MECHANIKY

FAKULTA STAVEBNÍ
INSTITUTE OF STRUCTURAL MECHANICS

TENSILE STRENGTH OF FIBROUS YARNS AND COMPOSITES

DOCTORAL THESIS TREATISE
TEZE DOKTORSKÉ PRÁCE

AUTHOR ROSTISLAV RYPL
AUTOR PRÁCE

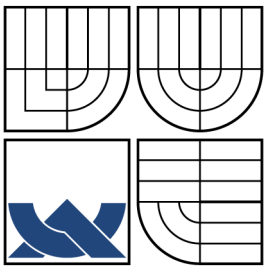

BRNO UNIVERSITY OF TECHNOLOGY
VYSOKÉ UČENÍ TECHNICKÉ V BRNĚ

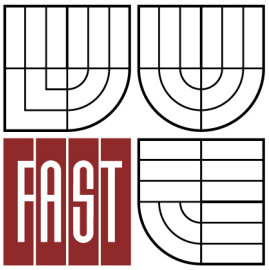

FACULTY OF CIVIL ENGINEERING
ÚSTAV STAVEBNÍ MECHANIKY

FAKULTA STAVEBNÍ
INSTITUTE OF STRUCTURAL MECHANICS

TENSILE STRENGTH OF FIBROUS YARNS AND COMPOSITES

TAHOVÁ PEVNOST VLÁKNITÝCH SVAZKŮ A KOMPOZITŮ

DOCTORAL THESIS TREATISE
TEZE DOKTORSKÉ PRÁCE

AUTHOR
AUTOR PRÁCE
ROSTISLAV RYPL

SUPERVISOR
VEDOUCÍ PRÁCE
prof. Ing. MIROSLAV VOŘECHOVSKÝ, Ph.D.

BRNO 2015

ABSTRACT

Technical textiles play a highly important role in today's material engineering. In fibrous composites, which are being applied in a number of industrial branches ranging from aviation to civil engineering, technical textiles are used as the reinforcing or toughening constituent. With growing number of production facilities for fibrous materials, the need for standardized and reproducible quality control procedures becomes urgent.

The present thesis addresses the issue of tensile strength of high-modulus multifilament yarns both from the theoretical and experimental point of view. In both these aspects, novel approaches are introduced. Regarding the theoretical strength of fibrous yarns, a model for the length dependent tensile strength is formulated, which distinguishes three asymptotes of the mean strength size effect curve. The transition between the model of independent parallel fibers applicable for smaller gauge lengths and the chain-of-bundles model applicable for longer gauge lengths is emphasized in particular. It is found that the transition depends on the stress transfer or anchorage length of filaments and can be identified experimentally by means of standard tensile tests at different gauge lengths.

In the experimental part of the thesis, the issue of stress concentration in the clamping has been addressed. High-modulus yarns with brittle filaments are very sensitive to stress concentrations when loaded in tension making the use of traditional tensile test methods difficult. A novel clamp adapter for the Statimat 4U yarn tensile test machine (producer: Textechno GmbH) has been developed and a prototype has been built. A test series comparing yarns strengths tested with the clamp adapter and with commonly used test methods has been performed and the results are discussed. Furthermore, they are compared with theoretical values using the Daniels' statistical fiber-bundle model.

KEYWORDS

fibrous yarns; probability and statistics, size-effect, tesile test of fibrous yarns

CONTENTS

1 INTRODUCTION

1.1 Motivation

The 20th century has witnessed an uprise of fibrous composites. Fibrous reinforcement has been used both for reinforcing polymer and metal matrices and toughening ceramic matrices. As the production of high modulus and high strength fibers – made of both ceramic and polymer materials – has grown in efficiency and thus has become more economic, the supreme properties of fibrous composites have been exploited by an ever wider range of industry branches. Having been discovered for aviation and sport, the domain of fibrous composites expanded over energy and automotive and, finally has reached civil engineering, where the strength and stiffness to weight and price ratio became interesting only at the end of the 1990s. There are in general three fundamental parts determining the mechanical behavior of fibrous composites:

1) fibers (reinforcing or toughening)
2) matrix (polymer, ceramic, metal)
3) interface between fibers and matrix

Even though there have been endless discussions on the hierarchy of priorities of these three components, it is probably most apt to conclude that each one plays a significant role with none of them being less important than the others.

For the most part, this thesis thoroughly examines the fibrous constituent separately. The understanding of the complex behavior of the fibrous constituent alone – fibers, bundles and yarns – provides much inside into the composite behavior and is of great significance for simulating the composite mechanics. However, in the last chapter, the interaction of short fiber bundles with cement-based matrix and the resulting composite called glass fiber reinforced concrete (GFRC) are analyzed.

Being a brittle material whose strength is governed by the weakest link, high-modulus fibers and fiber bundles exhibit various size-effects, which are in their elementary tendencies depicted in Fig. 1.1. On one hand, the tensile strength decreases with the gauge length of the fibrous material. On the other hand, the strength de-

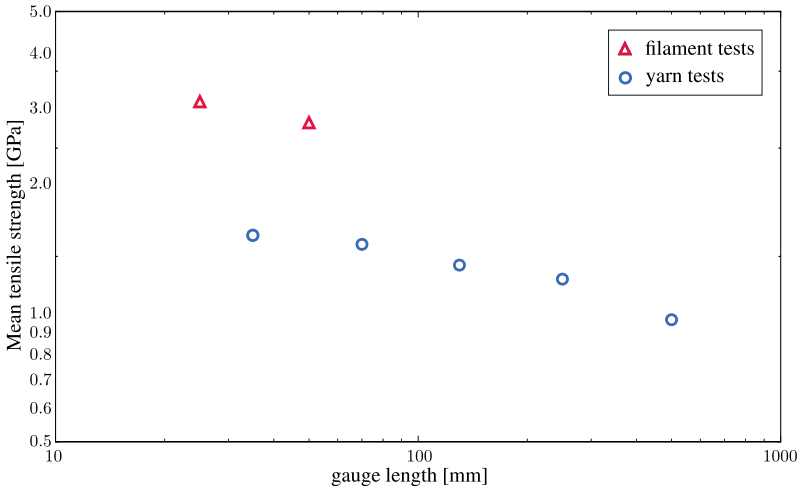

Fig. 1.1: Demonstration of size-effect in the tensile strength of high-modulus fibrous material: log-log plot of carbon filament and carbon yarn tensile strengths at various gauge lengths.

creases with the number of fibers in the bundle. In particular, the strength of a single fiber is on average about 20% higher than the strength of a multi-filament yarn. As shall be revealed in the body of the thesis, this tendency only applies for a range on gauge lengths and is violated above a transition threshold. Clearly, the tensile strength of fibrous materials is not a trivial quantity to identify and a number of mechanisms have to be understood in order to predict the tensile strength in a range extrapolated beyond experimentally measured data.

1.2 Goal setting

The main goals of this work can be summarized as follows:

(1) Provide a probabilistic model of the strength of high-modulus fibrous material for the complete range of gauge lengths.

(2) Address the clamping issue in tensile testing of fibrous yarns and propose an enhanced clamp device that reduces stress concentrations in the clamp region.

(2) Analyze and assess the behavior of short glass fiber reinforced cement-based matrix subjected to tensile loading from the probabilistic point of view.

2 STRESS TRANSFER LENGTH IN YARNS

The stress transfer length is a property of fibrous yarns, which governs their size effect behavior at longer gauge lengths, see Fig. 2.1. Therefore, it is highly important to identify this property in order to describe the tensile strength for an arbitrary length.

The key idea of the identification of the stress transfer length introduced in this thesis is to exploit the fact that the *in-situ* filament-filament interaction affects the length-dependent strength of the yarn (size effect curve). The effect of friction between filaments becomes significant when the specimen length is greater than the stress transfer length, i.e. the length at which a broken filament recovers its stress within the gauge length. Such a yarn structure becomes fragmented into a chain-of-bundles and behaves like a pseudo-composite and the slope of the size effect curve is decreased, see Fig. 2.1.

2.1 Model assumptions

The only source of randomness considered in the present model is the variability in local filament strength. Filaments respond elastically to tensile loading with brittle failure upon reaching their strength. The local random breaking strain ξ at a certain

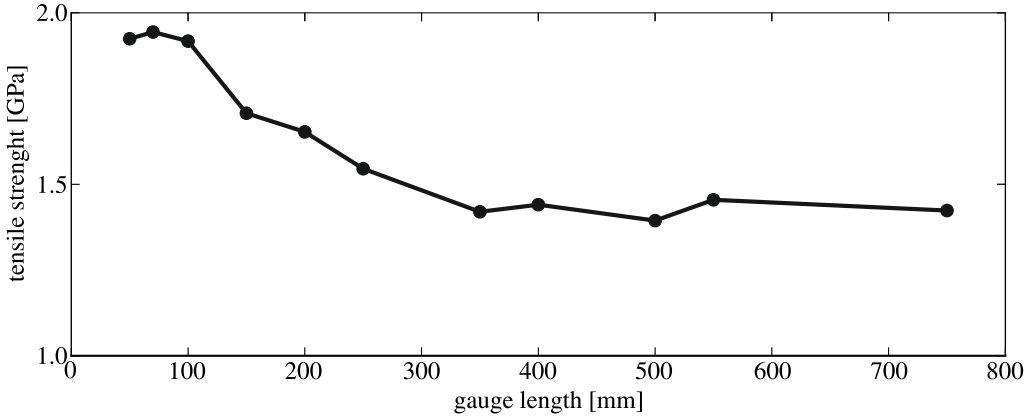

Fig. 2.1: Tensile strengths of Toho Tenax 1600 tex carbon yarns as measured at various gauge length.

point over the filament length is considered to follow the Weibull distribution:

$$F_\xi(\varepsilon) = \Pr\{\xi \leq \varepsilon\} = 1 - \exp\left[-\left\langle \frac{\varepsilon}{s} \right\rangle^m\right] \tag{2.1}$$

where s and m are the scale and shape parameter of the local distribution and ε is the imposed axial strain. The spatial distribution of the random strength along a filament has a length scale l_ρ at which the strength variability diminishes [28].

With these assumptions for a single filament a qualitative profile of the mean size effect curve of a fibrous yarn can be expected as shown in Fig. 2.2. Two types of mechanisms of load transfer can be distinguished depending on the yarn length. The two regions are separated by the effective bundle length (related to the stress transfer length) $l_\mathrm{b}^\star$ at which the fiber fragmentation can occur. In the range of gauge lengths $l < l_\mathrm{b}^\star$, the yarn behaves like a bundle of independent fibers [9, 8, 20, 24, 10] and in the range $l > l_\mathrm{b}^\star$, it behaves like a chain-of-bundles [14, 12, 13].

The transition zone from a bundle range to chain-of-bundles range is of special interest. The change in the slope of the size effect curve reveals the length $l_\mathrm{b}^\star$ at which the fragmentation starts. The idea of the present thesis is to exploit this fact in order to identify the effective bundle length $l_\mathrm{b}^\star$ within the tested yarn. The identification procedure searches for the intersection between the two branches of the mean size effect curve. The mathematical formulation of the two branches is summarized in the following two sections.

2.2 Bundle of parallel independent fibers

The mean strength of a single Weibullian filament is prescribed as

$$\mu_{\sigma_\mathrm{f}} = s_0 \cdot \left(\frac{l_0}{l}\right)^{-1/m} \cdot \Gamma\left(1 + \frac{1}{m}\right) \tag{2.2}$$

with s_0 and m denoting the scale and shape parameters of the Weibull distribution, respectively, and $\Gamma(\cdot)$ is the Gamma function [8]. The scale parameter s_0 is related to a reference length l_0. As pointed out in [28] the above power-law scaling predicts unlimited mean strength for $l \to 0$ and is therefore unrealistic. To impose an upper bound on the strength, a statistical length scale in the form of an autocorrelation

length of a random strength process along the filament has been introduced in [28]. With this in mind, the length-dependent mean filament strength given by Eq. (2.2) can be formulated with the variable l_ρ. The resulting form then includes the function $f_\rho(l_\rho, l)$ as:

$$\mu_{\sigma_\mathrm{f}} = s_0 \cdot f_\rho\left(l_\rho, l\right) \cdot \Gamma\left(1 + \frac{1}{m}\right) \tag{2.3}$$

The refined scaling function $f_\rho(l_\rho, l)$ accounting for the correlation length l_ρ has been suggested as either

$$f_\rho\left(l_\rho, l\right) = \left(\frac{l}{l_\rho} + \frac{l_\rho}{l_\rho + l}\right)^{-1/m} \tag{2.4}$$

or

$$f_\rho\left(l_\rho, l\right) = \left(\frac{l_\rho}{l_\rho + l}\right)^{1/m}. \tag{2.5}$$

Note that this length-scaling remains qualitatively unchanged for any arbitrary number of parallel filaments. Thus, in the sequel the length dependency of the scaling parameter within the range $l_\rho < l_\mathrm{b} < l_\mathrm{b}^\star$ (see Fig. 2.2) shall be represented by the scaling function

$$s_\mathrm{b} = s_0 \cdot f_\rho\left(l_\rho, l_\mathrm{b}\right). \tag{2.6}$$

In the limit of $l \gg l_\rho$, the scaling in Eqs. (2.4) and (2.5) recovers the classical Weibull length-dependency $f_\mathrm{W}\left(l\right) = \left(l_\rho/l\right)^{1/m}$. Such a decomposition of the length

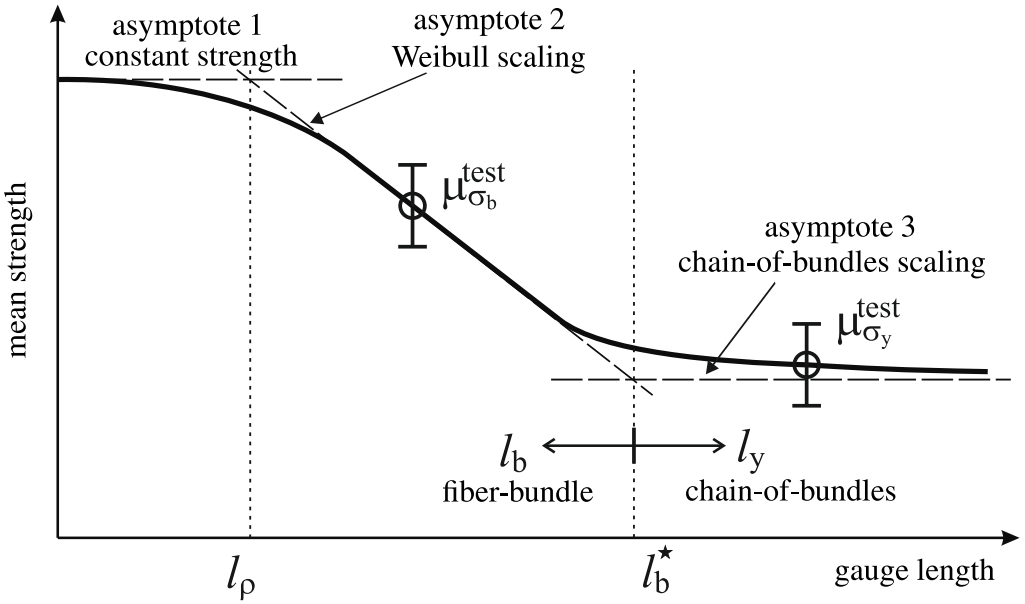

Fig. 2.2: Mean size-effect curve in log-log scale with three distinguished asymptotes

effect allows for a simple scaling of the mean value

$$\mu_{\sigma_1} = \mu_{\sigma_0} \cdot \frac{f_\rho(l_1)}{f_\rho(l_0)} \tag{2.7}$$

that shall be used later in the identification procedure.

The cumulative distribution function of a random per fiber bundle strength of a parallel set of filaments with independent identically distributed strength has been Derived by Daniels [9]. The resulting bundle strength approaches the Gaussian normal distribution as the number of filaments grows large ($n_\mathrm{f} \to \infty$). Based on Daniels' analysis, the expected asymptotic mean bundle strength μ_{σ_b} with Weibull fibers is related to the filament properties as

$$\mu_{\sigma_\mathrm{b}} = s_\mathrm{b} \cdot m^{-1/m} \cdot c_m \quad \text{with} \quad c_m = \exp\left(-\frac{1}{m}\right) \tag{2.8}$$

with s_b obtained using Equation (2.6). The standard deviation $\gamma_{\sigma_\mathrm{b}}$ is given as

$$\gamma_{\sigma_\mathrm{b}} = s_\mathrm{b} \cdot m^{-1/m} \sqrt{c_m \cdot (1 - c_m)}. \tag{2.9}$$

The decrease of the normalized mean bundle strength μ_{σ_b} with respect to the filament strength μ_{σ_f} is obvious from the comparison of Eqs. (2.8) and (2.2). In reality, bundles have a finite number of filaments n_f and the mean strength is thus only approaching the Daniels' asymptotic prediction. Both Smith and Daniels proposed ways to decrease the gap between the strength distribution of finite sized bundles and the asymptotic Daniels' normal approximation by adjusting μ_{σ_b} to $\mu_{\sigma_{\mathrm{b},\mathrm{n_f}}}$ [24, 10]. Both adjustments have a similar form so that only Smith's formula is written below for demonstration purposes:

$$\mu_{\sigma_{\mathrm{b},\mathrm{n_f}}} = \mu_{\sigma_\mathrm{b}} + n_\mathrm{f}^{-2/3} b \cdot \lambda. \tag{2.10}$$

In the case of Weibull filament distribution the parameter

$$b = s_\mathrm{b} \cdot m^{-1/m-1/3} \exp\left[-1/(3m)\right]$$

and the coefficient $\lambda = 0.996$. This correction shifts the mean value of the bundle strength. The standard deviation corresponding to μ_{σ_b} given by Eq. (2.9) is a fair approximation and does not need any further adjustment for a finite number of filaments n_f.

2.3 Chain of fiber bundles

The strength of a yarn (chain of fiber bundles) is governed by the weakest bundle and thus it is distributed as follows

$$H_{n_\mathrm{b},n_\mathrm{f}}(\varepsilon) = 1 - \left[1 - G_{n_\mathrm{f}}(\varepsilon)\right]^{n_\mathrm{b}}, \quad \varepsilon \geq 0 \tag{2.11}$$

with n_b being the number of serially coupled bundles.

The distribution of the chain-of-bundles strength can have different shapes depending on the ratio between the number of filaments n_f and number of bundles n_b [25, 27]. As known from the extreme value theory, the minimum of IID Gaussian variables, here representing the strength of a chain-of-bundles with dominating Gaussian distribution, approaches the Gumbel distribution [11] as $n_\mathrm{b} \to \infty$

$$H_{n_\mathrm{b},n_\mathrm{f}}(\varepsilon) = 1 - \exp\left[-\exp\left(\frac{\varepsilon - b_{n_\mathrm{b},n_\mathrm{f}}}{a_{n_\mathrm{b},n_\mathrm{f}}}\right)\right] \tag{2.12}$$

where

$$a_{n_\mathrm{b},n_\mathrm{f}} = \frac{\gamma_{\sigma_\mathrm{b}}}{\sqrt{2\omega}},$$

$$b_{n_\mathrm{b},n_\mathrm{f}} = \mu_{\sigma_\mathrm{b},n_\mathrm{f}} + \gamma_{\sigma_\mathrm{b}}\left[\frac{\ln(\omega) + \ln(4\pi)}{\sqrt{8\omega}} - \sqrt{2\omega}\right]$$

and $\omega = \ln(n_\mathrm{b})$. The mean value of yarn strength is then $\mu_{\sigma_\mathrm{y}} = b_{n_\mathrm{b},n_\mathrm{f}} - \eta \cdot a_{n_\mathrm{b},n_\mathrm{f}}$ and the median equals $b_{n_\mathrm{b},n_\mathrm{f}} + \ln(\ln(2)) \cdot a_{n_\mathrm{b},n_\mathrm{f}}$. Here, $\eta \approx 0.5772$ denotes the Euler-Mascheroni constant. The strength distribution given in Equation (2.12) is very accurate for a high number of filaments, n_f, and a number of bundles greater than approximately 300. For lower numbers of bundles $n_\mathrm{b} \in (1; 300)$, a cubic regression, which was proposed in [27], will be assumed for the mean chain-of-bundles strength. Using the constants introduced in Eq. (2.11), the cubic regression can be written as

$$\mu_{\sigma_\mathrm{y}} = \mu_{\sigma_\mathrm{b}} - \gamma_{\sigma_\mathrm{b}}\left(-0.007\omega^3 + 0.1025\omega^2 - 0.8684\omega\right), \tag{2.13}$$

where μ_{σ_b} and $\gamma_{\sigma_\mathrm{b}}$ are the bundle mean strength and standard deviation, respectively. This approximation describes the transition from the mean value of the Gaussian distribution of a single bundle to the mean value of the Gumbel distribution of a chain-of-bundles.

For the considered types of multifilament yarns consisting of several hundreds of filaments and a low number of bundles per meter (approximately 5 for AR-Glass, 2400 tex) it is sufficient to use the approximating Eq. (2.13) or the median value obtained from:

$$\sigma_y^{50} = \mu_{\sigma_{\mathrm{b,n_f}}} + \gamma_{\sigma_\mathrm{b}} \Phi^{-1}\left(1 - 0.5^{1/\mathrm{n_b}}\right). \tag{2.14}$$

Here, $\Phi^{-1}(\cdot)$ stands for the inverse standard Gaussian cumulative distribution function (percent point function) and $n_\mathrm{b} = l_\mathrm{y}/l_\mathrm{b}$ stands for the number of bundles the yarn consists of.

2.4 Evaluation of the effective bundle length

Let us assume that two sets of strength data $\mu_{\sigma_\mathrm{b}}^{\mathrm{test}}$ and $\mu_{\sigma_\mathrm{y}}^{\mathrm{test}}$ are available for two respective gauge lengths falling into the different length ranges defined in Sec. 2.1, i.e. $l_\mathrm{b}^{\mathrm{test}} < l_\mathrm{b}^\star$ and $l_\mathrm{y}^{\mathrm{test}} > l_\mathrm{b}^\star$. Apart from the known gauge lengths and the measured mean strengths, the knowledge of the Weibull modulus m and correlation length l_ρ are required. The estimation of the effective bundle length $l_\mathrm{b}^\star$ is then performed using the following procedure.

1. The mean strength $\mu_{\sigma_\mathrm{b}}^{\mathrm{test}}$ estimated as the average strength for the length $l_\mathrm{b}^{\mathrm{test}}$ is substituted into Eqs. (2.8) and (2.10) in order to obtain the scaling parameter s_b of the Weibull distribution for the tested length

$$s_\mathrm{b} = \mu_{\sigma_\mathrm{b}}^{\mathrm{test}} \cdot \left[m^{-1/m} \cdot \mathrm{c} + n_\mathrm{f}^{-2/3} \cdot\ m^{-(1/m+1/3)} \exp\left(-\frac{1}{3m}\right)\lambda\right]^{-1}. \tag{2.15}$$

2. With the scaling parameter s_b at hand, the corresponding standard deviation $\gamma_{\sigma_\mathrm{b}}$ is evaluated using Equation (2.9).
3. The obtained bundle characteristics are scaled to the unknown length $l_\mathrm{b}^\star$ using Eq. (2.7) and exploiting the fact that the standard deviation (as well as every quantile) scales identically with the mean value:

$$\mu_{\sigma_\mathrm{b}}^\star = \mu_{\sigma_\mathrm{b}}^{\mathrm{test}} \cdot \frac{f\left(l_\mathrm{b}^\star\right)}{f\left(l_\mathrm{b}^{\mathrm{test}}\right)} \ \text{ and } \ \gamma_{\sigma_\mathrm{b}}^\star = \gamma_{\sigma_\mathrm{b}}^{\mathrm{test}} \cdot \frac{f\left(l_\mathrm{b}^\star\right)}{f\left(l_\mathrm{b}^{\mathrm{test}}\right)}.$$

4. The chaining effect involved in the experimental data is now expressed using Equation (2.13) for the unknown bundle length $l_\mathrm{b}^\star$ as

$$\mu_{\sigma_\mathrm{y}}^{\mathrm{test}} = \mu_{\sigma_\mathrm{b}}^\star(l_\mathrm{b}^\star) - \gamma_{\sigma_\mathrm{b}}^\star\left(-0.007\omega_\star^3(l_\mathrm{b}^\star) + 0.1025\omega_\star^2(l_\mathrm{b}^\star) - 0.8684\omega_\star(l_\mathrm{b}^\star)\right) \tag{2.16}$$

where $\omega_\star$ represents the logarithm of the number of bundles in series $\omega_\star = \ln\left(l_\mathrm{y}^\mathrm{test}/l_\mathrm{b}^\star\right)$. The non-linear implicit Eq. (2.16) is then solved for $l_\mathrm{b}^\star$ using standard root finding algorithms.

In order to demonstrate the identification procedure on real data, two test series with different yarn types (carbon and AR-glass) have been conducted. The results of the evaluation of the effective stress transfer length are described in the full length version of this thesis.

2.5 Conclusions

The known aspect of length dependency of the tensile strength of fibrous yarns has been investigated and a model has been developed with two distinguished modes of mechanical behavior. These two modes represent the asymptotic behavior for short and long yarns.

Based on this idea, a method has been proposed to identify the transition length marking the 'effective bundle length'. With the use of a set of standard yarn tensile tests at different gauge lengths and an analytical model of the mean size effect curve, the inter-filament frictional interaction can be indirectly identified with a moderate effort.

3 TENSILE TESTING OF YARNS

3.1 Introduction

In order to validate any model of tensile strength of high-modulus multifilament yarns, an appropriate tensile test device has to be used for the experiments. The steadily growing application of technical yarns has evoked intensive efforts to improve the quality and reproducibility of strength characterization for this type of material [2, 22]. In contrast to traditional yarn materials like cotton and polyester, high-modulus yarns made of glass, carbon, aramid or UHMPE are very sensitive to stress concentrations due to their brittleness when loaded in tension. At the same time, they exhibit a pronounced strength size effect due to the presence of randomly distributed flaws along the yarn. Both these properties make the use of traditional setups for yarn tensile testing difficult.

Two categories of methods that are currently being used for introducing the tensile load into a high-modulus multifilament yarn in order to measure its tensile strength are outlined below. The main advantages and disadvantages of these commonly used methods are briefly summarized in Tab. 3.1.

3.1.1 Load transfer via deflection and friction

The first category uses mechanical fixing clamps and an additional deflection of the yarn which introduces the load to the yarn through friction. The deflection reduces the force which has to be taken up by the fixing clamps. An example of this method is the test with capstan grips [2, 1, 3] where the yarn is deflected or twisted around a spool, see Fig. 3.1a.

In some cases, the tests are semi or even fully automatic (Statimat 4U with 'big bollards', Textechno GmbH) which is a great advantage of this test method. However, the method also has some disadvantages. Due to the radii of the deflection elements, the minimum test length of the specimen is limited. Furthermore, the test length of the yarn is not precisely defined since the force is introduced over a certain length at the deflection elements. Since the yarn strength is length-dependent, the

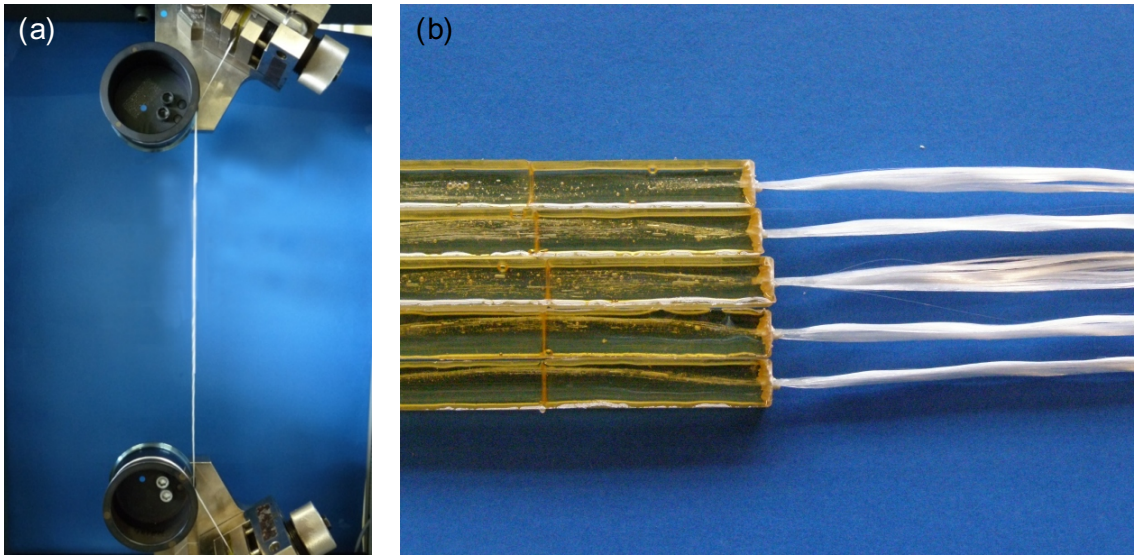

Fig. 3.1: Yarn tensile test with capstan grips – Zwick Roell AG (a); embedding the porters in resin (b) – specimens can be tested with any tensile test machine (ITA, RWTH university, Aachen, Germany

test length needs to be known for the interpretation of the yarn tensile properties. The main disadvantage, however, is the non-uniformly distributed stress among filaments. This issue arises because filaments directly contacting the spool carry more of the introduced load.

3.1.2 Load transfer via resin porters

The second category of testing methods uses resin blocks to embed the yarn end and introduce the load (Fig. 3.1b) [22, 7]. The main advantage of these methods is the relatively well-defined test length and the uniform load introduction at large test lengths and the disadvantage is the very time consuming sample preparation

Tab. 3.1: State of the art for tensile test methods.

method	gauge length	load introduction	specimen preparation
capstan grips	not accurately defined	non-uniform	automatic
resin porters	defined gauge length	uniform	time consuming

which is also biased by the human factor.

3.2 New tensile test device

The newly developed tensile test device – a clamp adapter for the tensile test machine Statimat 4U (referred to as 'Statimat 4U adapter' further in the text) – significantly reduces the problem of stress concentration in the clamps. On the other hand, compared to the current tensile test methods, it enables the testing of yarns with precisely defined lengths so that the device can be used to measure the effect of yarn length on its strength, see Chapter 2.

The basic concept of the test set up is the separation of the clamping function from the stress homogenization function at the ends of the test length into two pairs of separate clamps controlled by separate pressure air circuits. Thanks to the introduction of the homogenizing clamp into the semi-automated Statimat 4U machine, several test series with a large number of samples for varied test lengths and yarn materials can be performed.

Tensile tests performed with the Statimat 4U adapter proceed in the following steps:

1.) The outer 'fixation clamps' (FCs) clamp the yarn with the pressure p_{FC} and introduce a fraction of the axial prestress force F_0 (see Fig. 3.2a).

2.) The yarn is laterally compressed by the inner 'homogenization clamps' (HCs) with soft polyurethane contact layers with the pressure p_{HC} which increases the inter-filament interaction within the yarn cross-section.

3.) An additional axial force F_{HC} is introduced by the homogenization clamp. In general F_{HC} is much smaller (e.g. 1/10) than the corresponding F_{FC} (see Fig. 3.2b).

3.) The axial load F_{FC} is increased while keeping the difference between F_{FC} and F_{HC} constant, i.e. the additional axial force F_{HC} is constant (see Fig. 3.2c).

This way the yarn is not damaged by the HCs defining the gauge length since the majority of the tensile force is introduced by the outer FCs. The HCs combine lateral pressure via a soft contact layer with a moderate axial force. The lateral

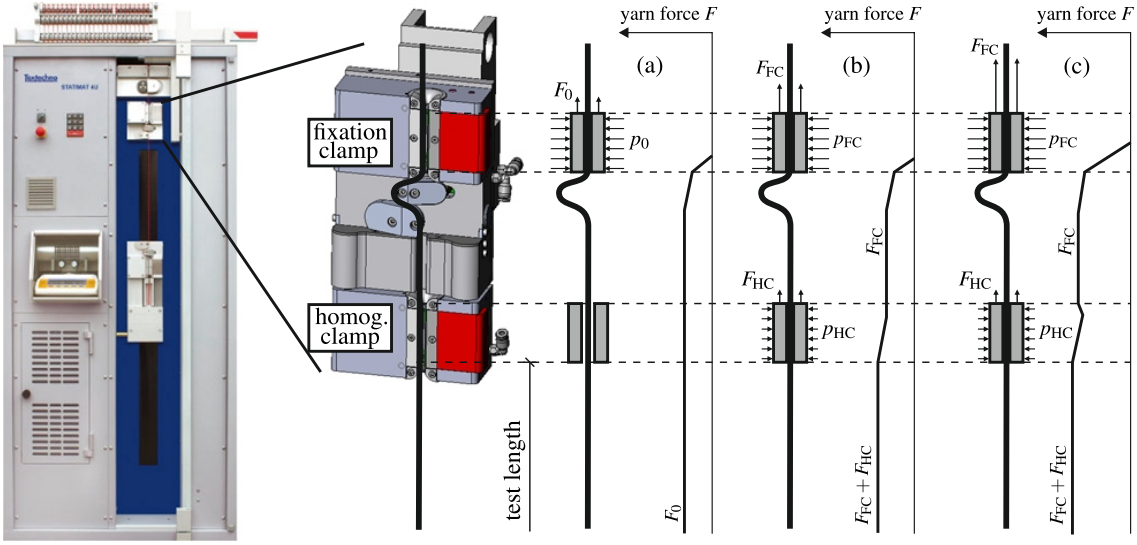

Fig. 3.2: Statimat 4U adapter with the newly developed clamp (detail): (a)-(c) phases of the tensile test with stress plotted along the tested yarn.

pressure p_{HC} homogenizes the stress in filaments by intensifying the inter-filament friction. At the same time, the additional axial force F_{HC} increases the probability of filament breaks within the gauge length and thus defines the gauge length. Note that the gauge length is, contrary to the deflection-friction tests, defined as the distance between the HCs. The deflection of the yarn around the bollards of the standard Statimat 4U machine (placed between the HCs and FCs in the adapter clamp version) has a similar function as the HCs — it takes up a part of the load due to friction and can be used in addition to the HC to diminish damage in the FCs.

In contrast to the standard clamping with bollards, the control parameters (e.g. the additional axial force F_{HC} introduced by the HCs, lateral pressure p_{FC} and p_{HC} of the respective FCs and HCs) of the adapter clamps can be freely adjusted to achieve optimal test setup for a given material. If, for example, a yarn consists of brittle filaments with rather large cross-sections, they will be more prone to rupture due to the lateral pressure of the homogenizing clamp which, in this case, should be kept low in order to best balance the trade-off between homogenization of stresses within the yarn cross-section and the initial filament damage.

3.3 Conclusions

The newly developed tensile test device Statimat 4U adapter largely diminishes stress concentrations in high-modulus yarns with brittle filaments and thus measures higher strengths than other tensile test methods. The full text version of the present thesis provides a validation of the new clamp device by comparing its performance and the performance of various reference methods. Furthermore, the measured yarn strengths are compared with the theoretical yarn strength derived in Chapter 2. Both the comparative experiment and the theoretical model confirm the better performance of the new device with a high statistical significance.

4 GLASS FIBER REINFORCED CONCRETE

4.1 Introduction

Glass fibers as reinforcement in cement-based matrix were first utilized in the 1960s in Russia [5]. A further major step towards glass fiber reinforced concrete (GFRC or GRC) is due to the company Owens Corning which developed alkali-resistant (AR) glass by increasing the content (>16%) of zirconia [29] in the material. This enhancement allowed for the production of a durable high-performance cement-based composite, which has been used in various modifications in structural and military engineering since [4, 21].

Each of the AR-glass fibers is a bundle of (typically 50 to 400) monofilaments which are bonded together by a sizing material. When bridging a crack, these filaments debond and rupture or are being pulled out and thus increase the toughness of the cement-based composite [18]. Moreover, the short dispersed fibers increase the first cracking stress and, above a critical volume fraction threshold, the ultimate tensile strength. These features together with the enhanced durability make the use of GFRC an alternative to traditional steel fiber reinforced concrete (FRC). However, the bridging mechanism is far more complex than in FRC.

Once a crack forms in the matrix, the glass fibers bridging the crack act against further crack opening by stretching and pullout. During this process, some filaments are completely pulled out while others rupture. The mechanism exhibits random features that can be divided into three scales:

1) At the micro scale, individual filaments within a bundle experience random interface shear flow depending on their position within the bundle and thus on the penetration of the matrix into the bundle core. A second source of randomness at the micro scale is the fiber strength that is determined by the weakest flaw in the material structure.
2) At the meso scale, individual bridging fibers are randomly oriented and positioned within the composite domain. This randomness causes variability in the bridging force due to snubbing and non-uniform pullout lengths [17]

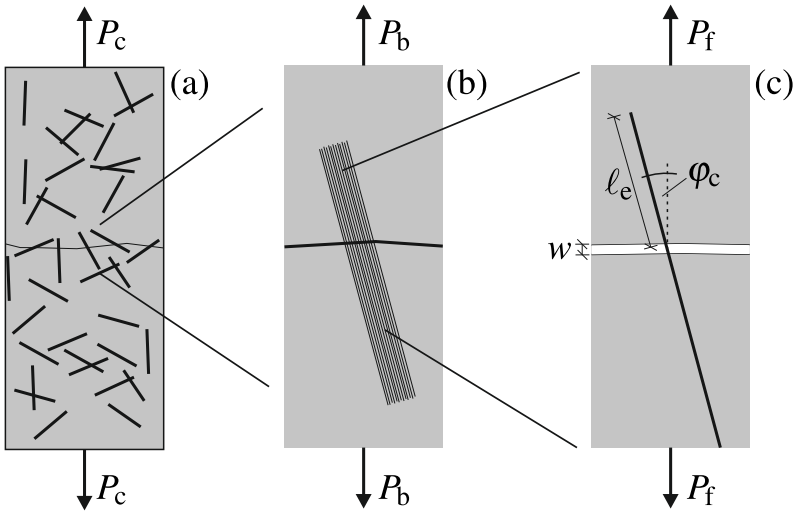

Fig. 4.1: Multiscale approach to the modeling of GFRC: (a) composite crack bridge with multiple filament bundles; (b) filament bundle; (c) single filament considered independently from the bundle.

3) At the macro scale, the overall number of fibers bridging a crack is a random variable that depends on the specimen geometry, fiber geometry and fiber volume fraction.

A model that considers these sources of random effects and reflects the complexity and unique bridging mechanism of the short glass fiber bundles does not exist to date.

4.2 Probabilistic model

The semi-analytical probabilistic model is limited to uniaxial tensile loading of a composite with discrete, planar matrix cracks and mechanically independent fibers. The mechanical independence of fibers is provided if matrix deformations are much lower than the fiber deformations i.e. the matrix stiffness $E_m(1 - V_f) \gg E_f V_f$ is much higher than that of the fibers. Here, E_m and E_f are the matrix and fiber elastic moduli, respectively, and V_f is the fiber volume fraction.

4.2.1 Single filament

Let us assume that the bridging action of a single filament with embedded length ℓ_e and inclination angle φ_c (with respect to the crack plane normal) is provided in the form

$$P_\mathrm{f} = f(w, \ell_\mathrm{e}, \varphi_\mathrm{c}, \boldsymbol{\theta}_\mathrm{r}, \boldsymbol{\theta}_\mathrm{d}), \tag{4.1}$$

where P_f is the bridging force, w is the crack opening, $\boldsymbol{\theta}_\mathrm{d}$ is a vector of deterministic parameters and $\boldsymbol{\theta}_\mathrm{r}$ a vector of random variables defined over the sampling space Ω_r with the corresponding joint distribution function G_{Ω_r}. The mean force transmitted by a filament within a bundle bridging a matrix crack is

$$\mu_{P_\mathrm{f}}(w, \ell_\mathrm{e}, \varphi_\mathrm{c}) = \mathrm{E}_{\Omega_\mathrm{r}}[P_\mathrm{f}] \tag{4.2}$$

with $\mathrm{E}_\Omega[\mathbf{X}]$ being the expectation operator applied to the random variable $\mathbf{X}$ defined over the sampling space Ω with the joint probability distribution function $G_\Omega(\mathbf{X})$, i.e.

$$\mathrm{E}_\Omega[\mathbf{X}] = \int_\Omega \mathbf{X}\,\mathrm{d}G_\Omega(\mathbf{X}). \tag{4.3}$$

The variance of the filament bridging force is given by

$$\sigma^2_{P_\mathrm{f}}(w, \ell_\mathrm{e}, \varphi_\mathrm{c}) = \mathrm{D}_{\Omega_\mathrm{r}}[P_\mathrm{f}], \tag{4.4}$$

with $\mathrm{D}_\Omega[\mathbf{X}]$ being the variance operator applied to the random variable $\mathbf{X}$ defined over the sampling space Ω with the joint probability distribution function $G_\Omega(\mathbf{X})$, i.e.

$$\mathrm{D}_\Omega[\mathbf{X}] = \mathrm{E}_\Omega[\mathbf{X}^2] - \mathrm{E}_\Omega[\mathbf{X}]^2 = \int_\Omega \mathbf{X}^2\,\mathrm{d}G_\Omega(\mathbf{X}) - \mathrm{E}_\Omega[\mathbf{X}]^2. \tag{4.5}$$

4.2.2 Filament bundle

Given the number of filaments in a bundle, n_f, the force transmitted by the whole bundle reads

$$P_\mathrm{b} = \sum_{i=1}^{n_\mathrm{f}} P_\mathrm{f}(w, \ell_\mathrm{e}, \varphi_\mathrm{c}, \boldsymbol{\theta}_{\mathrm{r},i}, \boldsymbol{\theta}_\mathrm{d}), \tag{4.6}$$

where $\boldsymbol{\theta}_{\mathrm{r},i}$ is the vector of parameters obtained as the i^th sample from the sampling space Ω_r of the random variables $\boldsymbol{\theta}_\mathrm{r}$. Since the inclinations and embedded lengths of the bridging bundles will be random, the φ_c and ℓ_e parameters are to be treated

as random variables. Their sampling space will be referred to as Ω_φ. The mean bridging force transmitted by a bundle has the form

$$\mu_{P_\mathrm{b}}(w) = \mathrm{E}_{\Omega_\varphi \Omega_\mathrm{r}}[P_\mathrm{b}] = n_\mathrm{f} \mathrm{E}_{\Omega_\varphi \Omega_\mathrm{r}}[P_\mathrm{f}]. \tag{4.7}$$

For the variance of the bundle bridging force, we have to use the law of total variance, which states

$$\mathrm{D}[Y] = \mathrm{E}[\mathrm{D}(Y|X)] + \mathrm{D}[\mathrm{E}(Y|X)]. \tag{4.8}$$

When this law is applied to the present case, $(Y|X)$ is substituted by $P_\mathrm{b}(w, \ell_\mathrm{e}, \varphi_\mathrm{c}, \boldsymbol{\theta}_\mathrm{d}|\boldsymbol{\theta}_\mathrm{r})$. We can alternatively express the conditional probability by explicitly writing the integration domain for individual statistical operators in the equation. With this notation, the variability of the randomly oriented filament bundle with random embedded length reads:

$$\begin{aligned} \sigma^2_{P_\mathrm{b}}(w) &= \mathrm{E}_{\Omega_\phi}\left[\mathrm{D}_{\Omega_\mathrm{r}}(P_\mathrm{b})\right] + \mathrm{D}_{\Omega_\phi}\left[\mathrm{E}_{\Omega_\mathrm{r}}(P_\mathrm{b})\right] \\ &= n_\mathrm{f}^2 \left(\mathrm{E}_{\Omega_\phi}[\mathrm{D}_{\Omega_\mathrm{r}}(P_\mathrm{f})] + \mathrm{D}_{\Omega_\phi}[\mathrm{E}_{\Omega_\mathrm{r}}(P_\mathrm{f})]\right). \end{aligned} \tag{4.9}$$

where we do not explicitly write out the dependencies of P_f on its parameters.

4.2.3 Multiple bundles

Let us now introduce the variable n_b, which stands for the number of bundles (chopped strands) bridging a matrix crack. In a composite with randomly dispersed fiber bundles, n_b will be a random variable with sampling space Ω_b. The total force transmitted by all n_b bundles can be written as

$$P_\mathrm{c} = \sum_{j=1}^{n_\mathrm{b}} \sum_{i=1}^{n_\mathrm{f}} P_\mathrm{f}(w, \ell_{\mathrm{e},j}, \varphi_{\mathrm{c},j}, \boldsymbol{\theta}_{\mathrm{r},ij}, \boldsymbol{\theta}_\mathrm{d}) = \sum_{j=1}^{n_\mathrm{b}} P_{\mathrm{b},j}, \tag{4.10}$$

where $\ell_{\mathrm{e},j}$ and $\varphi_{\mathrm{c},j}$ are the j^{th} samples from the Ω_φ sampling space, the vector $\boldsymbol{\theta}_{\mathrm{r},ij}$ is the ij^{th} sample from the sampling space Ω_r and $P_{\mathrm{b},j}$ can be expressed as

$$P_{\mathrm{b},j} = \sum_{i=1}^{n_\mathrm{f}} P_\mathrm{f}(w, \ell_{\mathrm{e},j}, \varphi_{\mathrm{c},j}, \boldsymbol{\theta}_{\mathrm{r},ij}, \boldsymbol{\theta}_\mathrm{d}). \tag{4.11}$$

The mean force resulting from the bridging action of randomly dispersed short fiber bundles has the form

$$\begin{aligned} \mu_{P_\mathrm{c}}(w) &= \mathrm{E}_{\Omega_\mathrm{b}\Omega_\varphi,\Omega_\mathrm{r}}[P_\mathrm{c}] = \mathrm{E}_{\Omega_\mathrm{b}}[n_\mathrm{b}]\, \mu_{P_\mathrm{b}}(w) \\ &= \mathrm{E}_{\Omega_\mathrm{b}}[n_\mathrm{b}]\, n_\mathrm{f}\, \mathrm{E}_{\Omega_\varphi \Omega_\mathrm{r}}[P_\mathrm{f}]. \end{aligned} \tag{4.12}$$

Applying the law of total variance according to Eq. (4.8) with $P_{\mathrm{c}}(w, \ell_{\mathrm{e}}, \varphi_{\mathrm{c}}, \boldsymbol{\theta}_{\mathrm{r}}, \boldsymbol{\theta}_{\mathrm{d}}|n_{\mathrm{b}})$ substituted for $(Y|X)$, the variance of the crack bridging force P_{c} is obtained as

$$\begin{aligned}\sigma^2_{P_{\mathrm{c}}}(w) &= \mathrm{D}_{\Omega_{\mathrm{b}}\Omega_{\varphi}\Omega_{\mathrm{r}}}[P_{\mathrm{c}}] = \mathrm{D}_{\Omega_{\mathrm{b}}\Omega_{\varphi}\Omega_{\mathrm{r}}}\left[\sum_{j=1}^{n_{\mathrm{b}}} P_{\mathrm{b},j}\right] \\ &= \mathrm{E}_{\Omega_{\mathrm{b}}}\left[\mathrm{D}_{\Omega_{\varphi}\Omega_{\mathrm{r}}}\left(\sum_{j=1}^{n_{\mathrm{b}}} P_{\mathrm{b},j}\middle| n_{\mathrm{b}}\right)\right] + \mathrm{D}_{\Omega_{\mathrm{b}}}\left[\mathrm{E}_{\Omega_{\varphi}\Omega_{\mathrm{r}}}\left(\sum_{j=1}^{n_{\mathrm{b}}} P_{\mathrm{b},j}\middle| n_{\mathrm{b}}\right)\right]\end{aligned} \tag{4.13}$$

Exploiting the independence of P_{b} and n_{b}, Eq. (4.13) can be simplified to

$$\begin{aligned}\sigma^2_{P_{\mathrm{c}}}(w) &= \mathrm{E}_{\Omega_{\mathrm{b}}}\left[n_{\mathrm{b}} \cdot \mathrm{D}_{\Omega_{\varphi}\Omega_{\mathrm{r}}}\left(P_{\mathrm{b}}\right)\right] + \mathrm{D}_{\Omega_{\mathrm{b}}}\left[n_{\mathrm{b}} \cdot \mathrm{E}_{\Omega_{\varphi}\Omega_{\mathrm{r}}}\left(P_{\mathrm{b}}\right)\right] \\ &= \mathrm{E}_{\Omega_{\mathrm{b}}}[n_{\mathrm{b}}] \cdot \mathrm{D}_{\Omega_{\varphi}\Omega_{\mathrm{r}}}\left[P_{\mathrm{b}}\right] + \mathrm{D}_{\Omega_{\mathrm{b}}}[n_{\mathrm{b}}] \cdot \left(\mathrm{E}_{\Omega_{\varphi}\Omega_{\mathrm{r}}}\left[P_{\mathrm{b}}\right]\right)^2.\end{aligned} \tag{4.14}$$

In order to evaluate the statistical moments of the bridging response, the distribution functions of the random variables need to be known. The derivation of distribution functions for individual random variables is out of the scope of the present publication so that we refer to [23] for the distribution of the strength of a brittle fiber in composite and the bond strength distribution. The distribution of the number of dispersed short fibers bridging a planar matrix crack is in detail dealt with in [26].

4.3 Discrete model

The discrete model developed by John E. Bolander at UC Davis [6] is introduced and used as reference for the probabilistic model described above. In the discrete model, fiber and matrix phase models are both based on a lattice model. The matrix phase is represented by a set of randomly distributed nodes which are interconnected by springs and kinematic constraints. This nodal set for the matrix phase has lattice topology and material properties by the Delaunay/Voronoi tessellations which enable the discretized matrix phase to behave in an elastically homogeneous fashion (Fig. 4.2a). As shown Fig. 4.2b, the matrix element is defined according to the rigid-body-spring concept [6]. The linear and rotational zero-size springs are formed at the centroid C of the area A_{ij} of the Voronoi facet common to nodes i and j. The spring set is constrained to nodes i and j via rigid arm constraints.

The fiber phase can be discretized within the computational domain irrespective of the background lattice representing the matrix [15]. A fiber element is defined

wherever a fiber passes through the Voronoi facet A_{ij} associated with a matrix element (Fig. 4.2c). In the semi-discrete fiber model, a linear zero-size spring for the fiber reinforcement is positioned at the intersection point I and aligned with the fiber path. The spring is linked to the associated two nodes i and j through rigid-arm constraints similar to the rigid-body-spring construction of the matrix elements. The semi-discrete modeling of fibers is computationally efficient, contrary to the fully-discrete fiber modeling in which a fiber is discretized as a series of the frame elements with additional nodal degrees of freedom and its elements are linked to the associated nodes via an ordinary bond link. This feature of the semi-discrete fiber model enables simulations with large numbers of fibers.

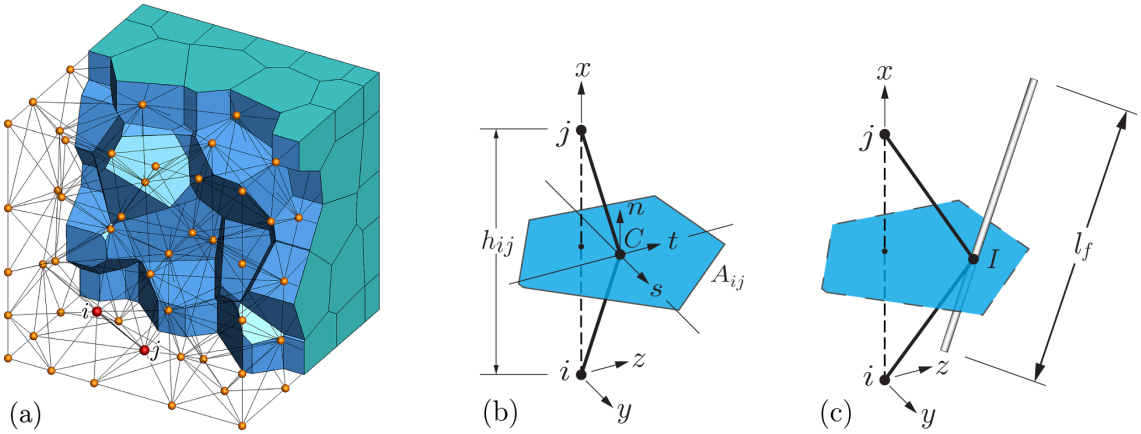

Fig. 4.2: Lattice discretization of fiber reinforced concrete: (a) Delaunay/Voronoi tessellations of material domain; (b) matrix element ij defined by facet centroid C; and (c) fiber element associated with intersection point I.

4.4 Computational example

Having formulated the modeling framework for GFRC in two alternatives, we can proceed to a computational example, which compares the two approaches. Both models require an independent micromechanical model of a fiber bridging action. For this purpose, we apply the analytical form due to [19] with snubbing and spalling effects according to [16]. For reasons of brevity and readability, we simplify the

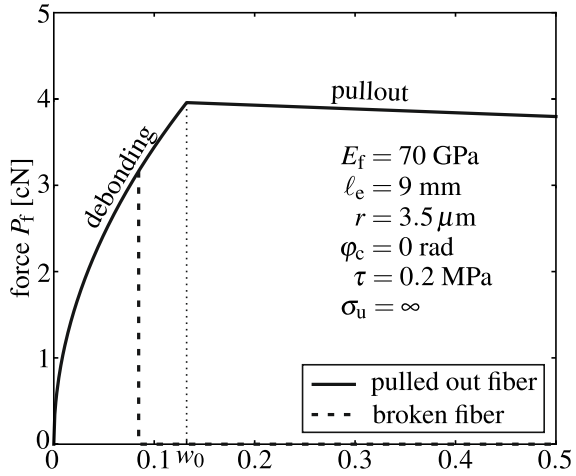

Fig. 4.3: Analytical model of a single fiber bridging action due to Naaman et al. [19].

general expressions by assuming a perfectly plastic (frictional) bond with infinite initial stiffness and constant bond strength. With these assumptions, the resulting form for a filament bridging action in the debonding phase reads

$$F_{\mathrm{f,deb}}(w, \sigma_{\mathrm{u}} = \infty) = A_{\mathrm{f}} \sqrt{\frac{2E_{\mathrm{f}}\tau w}{r}} \cdot \exp\left(f\varphi_{\mathrm{c}}\right) \cdot \left(\cos\varphi_{\mathrm{c}}\right)^{s} \tag{4.15}$$

with E_{f}, A_{f} and r being the filament modulus of elasticity, cross-sectional area and radius, respectively, τ denoting the bond strength, f the snubbing coefficient and s the spalling coefficient. When the fiber is fully debonded along the embedded length ℓ_{e}, the pullout stage starts. Again, for reasons of brevity, we ignore any hardening or softening during the pullout stage and write the bridging force during the pullout stage simply as

$$F_{\mathrm{f,pull}}(w, \sigma_{\mathrm{u}} = \infty) = 2\pi r\tau(\ell_{\mathrm{e}} + w_0 - w) \cdot \exp\left(f\varphi_{\mathrm{c}}\right) \cdot \left(\cos\varphi_{\mathrm{c}}\right)^{s} \tag{4.16}$$

with w_0 being the crack opening at the transition between the debonding and pullout stage. It can be obtained by formulating the continuity condition

$$F_{\mathrm{f,deb}}(w_0) = F_{\mathrm{f,pull}}(w_0) \rightarrow w_0 = \frac{2\ell_{\mathrm{e}}^2\tau}{rE_{\mathrm{f}}}. \tag{4.17}$$

In both Eq. (4.15) and Eq. (4.16), the assumption was that fibers have an infinite strength $\sigma_{\mathrm{u}} = \infty$. If we now include the possibility of fiber rupture, we have to

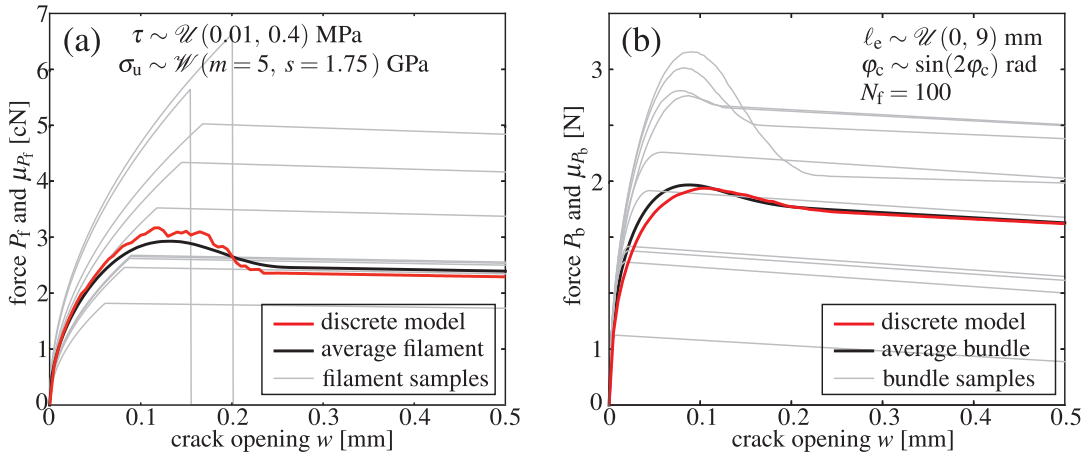

Fig. 4.4: Computational example performed with the present modeling framework: (a) single filament bridging responses (gray curves) sampled from the sampling space of random variables ($\tau \sim$ uniform distribution between 0.01 and 0.4 MPa and $\sigma_u \sim$ Weibull distribution with shape $m = 5$ and scale $s = 1.75$ GPa) and mean filament response (black curve); (b) filament bundle responses sampled from the sampling space of random variables ($\varphi_c \sim \sin(2x)$ distribution and $\ell_e \sim$ uniform distribution between 0 and 9 mm) and mean bundle response (black curve).

multiply the fiber force in the debonding phase by $H(\sigma_u - \sigma_f)$, where σ_f denotes the fiber stress and $H(\cdot)$ the Heaviside step function defined as

$$H(x) = \begin{cases} 0 & : x < 0 \\ 1 & : x \geq 0. \end{cases} \tag{4.18}$$

The filament force in the debonding stage then becomes

$$F_{f,deb}(w) = A_f \sqrt{\frac{2E_f \tau w}{r}} \cdot \exp(f\varphi_c) \cdot (\cos\varphi_c)^s \cdot H(\sigma_u - \sigma_f) \tag{4.19}$$

with

$$\sigma_f = \frac{F_{f,deb}(w, \sigma_u = \infty)}{A_f}. \tag{4.20}$$

In a similar manner, the pullout force has to be multiplied by a Heaviside function which ensures that fibers have not ruptured at their peak stress during the debonding so that

$$F_{f,pull}(w) = 2\pi r \tau (\ell_e + w_0 - w) \cdot \exp(f\varphi_c) \cdot (\cos\varphi_c)^s \cdot H(\sigma_u - \sigma_{f,max}), \tag{4.21}$$

where

$$\sigma_{\mathrm{f,max}} = \frac{2\pi r \tau \ell_{\mathrm{e}}}{A_{\mathrm{f}}}. \tag{4.22}$$

The complete filament bridging action (see Fig. 4.3) can be written as

$$P_{\mathrm{f}}(w) = F_{\mathrm{f,deb}}(w) \cdot H(w_0 - w) + F_{\mathrm{f,pull}} \cdot H(w - w_0). \tag{4.23}$$

An example of the filament bridging action is depicted in Fig. 4.4a for material parameters that correspond to AR-glass fibers with random τ distributed uniformly between 0.01 and 0.4 MPa and random fiber strength σ_{u} with Weibull distribution with shape parameter $k = 5$ and scale parameter $\lambda = 1.75$ GPa. The filaments are embedded perpendicular to the crack plane in this example. The figure shows samples from the distributions given by Eq. (4.23) and the mean filament response given by Eq. (4.2), which, multiplied by the number of filaments in a bundle, is the prediction of the response of a perpendicularly embedded filament bundle. The red curve is a single simulation of a bundle consisting of 100 filaments performed by the discrete model.

Fig.4.4b depicts the bridging force of a bundle consisting of $n_{\mathrm{f}} = 100$ filaments with random bond strength and fiber strength as in Fig. 4.4a but, additionally, the orientation angle and embedded length are considered as random variables. Random samples of such filament bundles and the mean bundle bridging force predicted by the probabilistic model with Eq. (4.7) are depicted. The red curve is the bridging force of $n_{\mathrm{b}} = 100$ bundles that are randomly oriented and positioned within the crack predicted by the discrete model.

4.5 Conclusions

Both the probabilistic and the discrete model are capable of simulating the crack bridging action of chopped AR-glass strands in a cement-based matrix. The probabilistic model is computationally very efficient and able to evaluate statistical moments of the response. However, the model formulation includes a number of assumption that make the model of use only for uniaxial tension in its current form.

The discrete model evaluates the response of the composite as a single sample. Therefore, repeated calculations would have to be performed when the variability was of interest. The discrete model, even though more computationally demanding, is much more robust than the probabilistic model. It is not limited to uniaxial tension and is therefore suitable for general purposes. Its comparison with the probabilistic model serves as a verification of the semi-discrete fiber bundle implementation.

REFERENCES

[1] A. Abdkader and P. Offermann. Textile Werkstoffe und Flächengebilde zur bautechnischen Verstärkung und Instandsetzung, Teil 1: Deformationskennwerte von AR-Glasfilamenten. *Technische Textilien*, H.4(43):265–266, 268–270, 2000.

[2] A. Abdkader and P. Offermann. Textile Werkstoffe und Flächengebilde zur bautechnischen Verstärkung und Instandsetzung, Teil 3: Deformationskennwerte von AR-Glasfilamenten. *Technische Textilien*, H.1(45):21–23, 2002.

[3] A. Abdkader and P. Offermann. Textile Werkstoffe und Flächengebilde zur bautechnischen Verstärkung und Instandsetzung, Teil 4: Einfluss der Prüfbedingungen und Schlichte auf die Deformationskennwerte von AR-Glasfilamentgarnen. *Technische Textilien*, H.3(45):154–156, 2002.

[4] H. Ball. 35 year review of the grc technology, equipment and markets. In *GRCA Congress*, Istanbul, 2011.

[5] K.L Biryukovich, Y. Biryukovich, and D.L Biryukovich. *Glass fibre reinforced cement*. CERTA Translation No. 12 Civil Engineering Research Assotiation, London, 1965.

[6] J.E. Bolander and N. Sukumar. Irregular lattice model for quasistatic crack propagation. *Physical Review B*, 71:094106, 2005.

[7] R. Chudoba, M. Vořechovský, V. Eckers, and Th. Gries. Effect of twist, fineness, loading rate and length on tensile bahavior of multifilament yarns (a multivariate study). *Textile Research Journal*, 77(11):880–891, 2007.

[8] B.D. Coleman. On the strength of classical fibres and fibre bundles. *Journal of Mechanics and Physics of Solids*, 7:60–70, 1958.

[9] H.E. Daniels. The statistical theory of the strength of bundles of threads. I. *Proceedings of the Royal Society of London. Series A, Mathematical and Physical Sciences*, 183(995):405–435, 1945.

[10] H.E. Daniels. The maximum of a gaussian process whose mean path has a maximum, with an application to the strength of bundles of fibres. *Advances in Applied Probability*, 21(2):315, Jun 1989.

[11] E. J. Gumbel. *Statistics of Extremes*. Columbia University Press, New York, 1958.

[12] D.G. Harlow and S.L. Phoenix. The chain-of-bundles probability model for the strength of fibrous materials I: Analysis and conjectures. *Journal of Composite Materials*, 12(2):195–214, 1978.

[13] D.G. Harlow and S.L. Phoenix. The chain-of-bundles probability model for the strength of fibrous materials II: a numerical study of convergence. *Journal of Composite Materials*, 12(3):314–334, 1978.

[14] D.G. Harlow, R.L. Smith, and H.M. Taylor. Lower tail analysis of the distribution of the strength of load-sharing systems. *Journal of Applied Probability*, 20(2):358–367, 1983.

[15] J. Kang, K. Kim, Y.M. Lim, and J.E. Bolander. Modeling of fiber-reinforced cement composites: Discrete representation of fiber pullout. *International Journal of Solids and Structures*, 51:1970–1979, 2014.

[16] Y. Lee, S.T. Kang, and J.K. Kim. Pullout behavior of inclined steel fiber in an ultra-high strength cementitious matrix. *Construction and Building Materials*, 24:2030–2041, 2010.

[17] V.C. Li, Y. Wang, and S. Backer. A micromechanical model of tension-softening and bridging toughening of short random fiber reinforced brittle matrix composites. *Journal of the Mechanics and Physics of Solids*, 39(5):607–625, 1991.

[18] B. Mobasher and S.P. Shah. Test parameters for evaluating toughness of glass fiber reinforced concrete panels. *Materials Journal*, 86:448–458, 1989.

[19] A.E. Naaman, G.G. Namur, J.M. Alwan, and H.S. Najm. Fiber pullout and bond slip. I: Analytical study. *Journal of Structural Engineering*, 117(9):2769–2790, 1991.

[20] S.L. Phoenix. Probabilistic strength analysis of fibre bundle structures. *Fibre Science And Technology*, 7:15 – 30, 1974.

[21] M.J. Roth, C.D. Eamon, T.R. Slawson, T.D. Tonyan, and A. Dubey. Ultra-high-strength, glass fiber-reinforced concrete: Mechanical behavior and numerical modeling. *ACI Materials Journal*, 2:185–194, 2010.

[22] A. Gries Roye and T. Three dimensional and online-shaped textile production with double needle bar raschel machines and weft insertion for concrete applications. *ACI Symposium Publication*, 244-CD:77 – 86, 2007.

[23] R. Rypl, R. Chudoba, A. Scholzen, and M. Vořechovský. Brittle matrix composites with heterogeneous reinforcement: Multi-scale model of a crack bridge with rigid matrix. *Composites Science and Technology*, 89:98–109, December 2013.

[24] R.L. Smith. The asymptotic distribution of the strength of a series-parallel system with equal load-sharing. *The Annals of Probability*, 10(1):137–171, 1982.

[25] R.L. Smith and S.L. Phoenix. Asymptotic distributions for the failure of fibrous materials under series-parallel structure and equal load-sharing. *Journal of Applied Mechanics*, 48:75 – 82, 1981.

[26] M. Vořechovský, V. Sadílek, and R. Rypl. Probabilistic evaluation of crack bridge performance in fiber reinforced composites. *Engineering mechanics*, 20(1):3–11, 2013.

[27] M. Vořechovský. Incorporation of statistical length scale into weibull strength theory for composites. *Composite Structures*, 92(9):2027–2034, 2010.

[28] M. Vořechovský and R. Chudoba. Stochastic modeling of multifilament yarns: II. random properties over the length and size effect. *International Journal of Solids and Structures*, 43(3-4):435–458, 2006.

[29] W. Wolf Warren. Glass fiber reinforced cement, 1975. US Patent 3,902,912.